Enzyme-functionalized biomimetic apatites: concept and perspectives in view of innovative medical approaches

**Christina G. Weber · Michaela Mueller · Nicolas Vandecandelaere ·
Iris Trick · Anke Burger-Kentischer · Tanja Maucher · Christophe Drouet**

Abstract Biomimetic nanocrystalline calcium-deficient apatite compounds are particularly attractive for the setup of bioactive bone-repair scaffolds due to their high similarity to bone mineral in terms of chemical composition, structural and substructural features. As such, along with the increasingly appealing development of moderate temperature engineered routes for sample processing, they have widened the armamentarium of orthopedic and maxillofacial surgeons in the field of bone tissue engineering. This was made possible by exploiting the exceptional surface reactivity of biomimetic apatite nanocrystals, capable of easily exchanging ions or adsorbing (bio)molecules, thus leading to highly-versatile drug delivery systems. In this contribution we focus on the preparation of hybrid materials combining biomimetic nanocrystalline apatites and enzymes (lysozyme and subtilisin). This paper reports physico-chemical data as well as cytotoxicity evaluations towards Cal-72 osteoblast-like cells and finally antimicrobial assessments towards selected strains of interest in bone surgery. Biomimetic apatite/enzyme hybrids could be prepared in varying buffers. They were found to be non-cytotoxic toward osteoblastic cells and the enzymes retained their biological activity (e.g. bond cleavage or antibacterial properties) despite the immobilization and drying processes. Release properties were also examined. Beyond these illustrative examples, the concept of biomimetic apatites functionalized with enzymes is thus shown to be useable in practice, e.g. for antimicrobial purposes, thus widening possible therapeutic perspectives.

C. G. Weber · M. Mueller · I. Trick · A. Burger-Kentischer ·
T. Maucher
Fraunhofer IGB Institute, Nobelstraße 12, 70569 Stuttgart,
Germany

C. G. Weber · T. Maucher
Institute of Interfacial Process Engineering and Plasma
Technology, University of Stuttgart, Nobelstraße 12,
70569 Stuttgart, Germany

N. Vandecandelaere · C. Drouet (✉)
CIRIMAT Carnot Institute, UMR CNRS/INPT/UPS 5085,
University of Toulouse, Ensiacet, 4 allée E. Monso,
31030 Toulouse Cedex 4, France
e-mail: christophe.drouet@ensiacet.fr

1 Introduction

Calcium phosphate apatite compounds, deriving from hydroxyapatite (HA), $Ca_{10}(PO_4)_6(OH)_2$, have been the object of many medically-oriented studies. Synthetic apatites, exhibiting variable reactivities and physico-chemical characteristics, may be produced by a variety of methods including wet chemical precipitations (see for example refs. [1, 2]), sol–gel [3], hydrothermal synthesis [4], mechanochemical synthesis [5], microwave processing [6], vapor diffusion [7], silica gel template [8], emulsion-based syntheses [9], electrospraying [10] The nucleation and growth of apatite on the surface of substrates immersed in supersaturated fluids (e.g. simulated body fluid) is also a way to obtain apatitic coverages (see for example Ref. [2]), although care should be taken in careful coating characterization for assessing its apatitic nature in all cases [11].

Nanocrystalline calcium phosphate apatites represent an appealing subclass of apatite compounds due to their peculiar features. They found applications not only in the field of bone regeneration [12–18] but also, more recently, in other domains such as cancer treatment or diagnosis [19–21]. This increased interest, especially noticeable during this last decade, most probably finds its origin in a better comprehension of their physico-chemical characteristics

and surface reactivity [22, 23], thus enabling one to exploit these materials more in depth. Also, these compounds—long considered as "laboratory curiosities" by some researchers—have been shown to be genuine material-making systems [15] capable of being processed and shaped, and are now accepted as a class of promising bio-active ceramics.

It has been established that, similarly to the mineral part of bone, synthetic calcium-deficient apatites prepared in close-to-biological conditions (low temperature, physiological pH) are constituted of nanocrystals involving an apatitic core covered by a calcium phosphate hydrated layer in which the constitutive mineral ions are found in non-apatitic chemical environments [18, 22–24]. These compositional, structural and microstructural analogies to bone apatite thus allow one to consider such systems as biomimetic to bone mineral. Since the overall 3D cohesion of such ionic crystals is mainly ensured by strong electrostatic forces between anions and cations, the nonstoichiometry character often observed for precipitated calcium-deficient apatites then leads to an increased solubility (or in turn greater resorption rate in vivo) thus enabling one to obtain resorbable bone-repair scaffolds. Also, the ions composing the non-apatitic surface layer were shown to be particularly labile [25] and can thus be exchanged, either during synthesis or at the occasion of post-synthesis steps, by biologically-active ions (e.g. Ca^{2+} may be substituted by Mg^{2+} or Sr^{2+} [23] in view of osteoporosis treatment), thus conferring additional bioactivity to these materials. In addition to the enrichment of biomimetic calcium-deficient apatites with selected biologically-relevant ions, the adsorption of organic (bio)molecules/drugs on the surface of apatite nanocrystals is another way to convey added functionalities to these systems [22]. For instance, associations with antibiotics, blood proteins, growth factors or else anticancer drugs have been reported in view of setting up advanced drug-loaded bioceramics [20, 22, 26–31]. In this view, nanocrystalline apatite-based systems and their reactivity thus differ from stoichiometric HA, which is often used in its calcined form leading to a limited bioactivity (low solubility, non-labile surface ions…). The high ion mobility found on the surface of calcium-deficient apatite nanocrystals may in particular be advantageously exploited for adsorptive as well as release properties [32].

Although the functionalization of apatite nanocrystals with a number of (bio)molecules has been the object of a great number of studies [27, 28, 30, 32–41], associations with enzymes has received less attention. In this regard, the interaction in solution of hydroxyapatite surfaces with lysozyme (often denoted "Lysozyme (LSZ)") has been the main reported example [42–50]. Authors converged to consider LSZ adsorption on apatites as mainly electrostatically-driven. The adsorption was found to be reversible with respect to dilution [42] and Langmuir-type isotherms were reported. The possibility to go one step further and prepare actual hybrid nano-apatite/enzyme *materials* (dry) to be used in medical applications was much less addressed though. Martins et al. [46] reported one case of chitosan scaffolds covered by a CaP coating, for which LSZ was incorporated with the goal to create pores in the chitosan matrix, but the direct preparation of biomimetic apatite/LSZ applicative materials has not been directly regarded to our knowledge. Furthermore, although Roger et al. [51] reported an inhibition of adherence of *Streptococcus mutans* on saliva-coated hydroxyapatite, the preservation and potential use of enzymatic activity (e.g. intrinsic antimicrobial properties) after enzyme immobilization/material processing steps have only rarely been explored. Yet, many biological processes are catalyzed by enzymatic processes and the ability to deliver particular enzymes to specific locations in vivo may appear as a clever way to speed up natural biological pathways or to intentionally provoke some in situ enzymatic activity [52–54]. Also, as mentioned above, selected enzymes exhibit intrinsic properties such as antimicrobialness (e.g. [51, 55]) that may be profitably exploited in medicine.

In this contribution we thus focused on a more "applicative" perspective, by the preparation of *biomimetic* calcium-deficient apatite/enzyme hybrid *materials* in direct relation with potential applications in medicine. Two types of "model" enzymes previously found to exhibit antibacterial properties (namely subtilisin [56] and the above-mentioned LSZ [57]) were employed here. The proteolytic enzyme subtilisin (a serine endopeptidase) is a protease secreted from many Bacillus species, which catalyzes the breakdown of proteins. Its interaction with apatites has apparently not been studied to this day. It is however largely used in various commercial applications such as cosmetics or food processing [56] in view of exploiting anti-biofouling/antibiofilm effects [58]. LSZ (a glycoside hydrolase), for which interactions with apatite surfaces have received some attention especially by studying in solution its adsorption process (see references mentioned above) is another natural antibacterial enzyme [59] found in a wide variety of organisms including birds, mammals, plants and insects, among others [60]. It is known to damage bacterial cell walls, especially for Gram-positive bacteria, by attacking peptidoglycans. It is naturally present in various secretions like tears, saliva, human milk and mucus, and plays a role in the innate immune system [59]. These features as well as the access to published data on the adsorption mechanism on (hydroxy)apatite (for which the biomimetic character was however not shown) made of LSZ a good candidate in this study, for going one step further and explore possible applicative antibacterial possibilities.

In this context, physico-chemical characteristics, osteoblast-type cell viability (cytotoxicity), as well as antibacterial assessments were examined in this paper after enzyme immobilization on *biomimetic nanocrystalline calcium-deficient apatites*, with the idea to underline applicative aspects. In particular, the preservation of enzymatic activity despite immobilization and drying processes was followed. These illustrative examples are thought to underline the promise of biomimetic apatite/enzyme associations in view of new therapeutic approaches.

2 Experimental

2.1 Synthesis of nanocrystalline calcium-deficient apatite substrates

The nanocrystalline calcium phosphate apatite samples used in this study were prepared by soft chemistry, via precipitation in aqueous medium at room temperature and in close-to-physiological pH (7.2). This pH value was ensured by an excess of phosphate ions in the medium, thus making it possible to avoid the addition of any foreign pH-buffering substance at the synthesis stage. The precipitation methodology involved calcium nitrate tetrahydrate (Merck Emsure grade, purity 99.0 %) as calcium source (aqueous solution A, with a calcium concentration of 0.3 M) and di-ammonium hydrogenphosphate (VWR Normapur grade, purity 99.0 %) as the phosphate source (solution B, orthophosphate concentration: 0.6 M). After rapidly pouring solution A into solution B and intimate mixing via stirring, at ambient temperature, the precipitating medium was left to mature for up to 6 days (aging in solution)—as stated in the text by the notation hap-Xd for a sample matured for X days—prior to filtration on Büchner funnel, thorough washing with deionized water, and freeze-drying leading to powder samples. Apatite pellets (typically 130 mg of powder, 13 mm diameter, 1 mm thick) were also prepared when needed, by uniaxial pressing of apatite powder (at least 40 MPa).

When mentioned in the text (release study), a commercial stoichiometric HA specimen (Alfa Aesar, Germany, CAS no. 12167-74-7) was also used for comparative assessments.

2.2 Physico-chemical characterization of the apatite substrates

Physico-chemical characteristics of apatite samples were drawn from complementary techniques. Structural features were investigated by X-ray diffraction (XRD) on an INEL 120 CPS diffractometer (cobalt radiation, $\lambda_{Co} = 1.78892$ Å). Mean crystallite dimensions were evaluated using Scherrer's formula. Fourier transform infrared (FTIR) spectra were recorded on a Nicolet 5700 spectrometer in the range 400–4,000 cm^{-1} (64 scans, resolution 4 cm^{-1}) in order to complete the structural analysis of the substrates.

Calcium and orthophosphate (PO_4^{3-} and HPO_4^{2-}) ionic contents were determined, after dissolution of the samples in perchloric acid, respectively by EDTA complexometry and by visible spectrophotometry (using the phoshpho–vanado–molybdenic complex, with $\lambda = 460$ nm) [61]. The relative uncertainty on calcium and phosphorus concentrations is evaluated to 0.5 %. The Ca/P atomic ratio of apatites was then derived from the result of these two analyses.

TEM observations were made on a JEOL—JEM1400 microscope, under a tension of 120 kV and a current of 76 µA. For sample preparation prior to TEM analysis, a low quantity of power was dispersed in ethanol before deposition on a copper grid and drying in air.

2.3 Association with enzymes (examples shown: subtilisin and lysozyme)

Subtilisin, a protease from *Bacillus Licheniformis*, was purchased from Sigma Aldrich, Germany (CAS number 9014-01-1, molecular weight 27 kDa). LSZ, arising from chicken egg white (CAS number 12650-88-3, molecular weight 16 kDa) was provided by Merck Chemicals Ltd., Nottingham, UK.

The adsorptive immobilization of the enzymes (subtilisin or LSZ, respectively) onto the apatites samples (as powders or pellets) was carried out by way of a three-step process: a first immersion step was processed by contacting the apatite samples with the corresponding enzyme, this immobilization step was then followed by methodical washing, and finally by a drying step.

The procedure used for subtilisin immobilization on apatite powders can be described as follows: 5 mL of subtilisin solution at a concentration of 2 mg ml^{-1} in either 1 M Tris buffer with 10 mM CaCl$_2$ (pH 7.8) or in 5 mM phosphate buffer with 0.3 mM CaCl$_2$ (pH 6.5) were added to 130 mg of apatite powder. The mixture was placed on a shaker at 4 °C for 24 h to allow the adsorption of the enzyme onto the apatite substrate. Previous work on the adsorption of proteins including enzymes (e.g. LSZ) on various solid surfaces had indeed shown that an incubation time of 20 h was appropriate to reach equilibrium (steady adsorption state) [62]. Subsequently the non-adsorbed subtilisin molecules were removed by repeated incubation with 5 mL of the respective buffer solution for at least 1 h at 4 °C on a shaker. For determining the end of washing and the amount of stably-adsorbed enzyme, the protein concentration was frequently measured in the supernatant by Bradford assays as described below.

Similarly, LSZ was immobilized on apatite samples as follows: after preparing the desired LSZ concentration in buffer solution [either 1 M Tris buffer with 10 mM $CaCl_2$ (pH 7.8) or 7.8 mM Citrate buffer (pH 6.5)], 50 mL of the solution were added to 13 g of apatite powder, which was again followed by an immersion period of 24 h at 4 °C with gentle shaking, washing in MilliQ water and freeze-drying for 16 h.

Enzyme immobilizations on apatite pellets were performed after pelletizing, leading to adsorption on the accessible pellet surface. In this case, 500 μL of buffer solution containing the enzyme was used per pellet of 130 mg.

The quantification of immobilized enzymes was determined by Bradford assay (BioRad, Germany), based on an absorbance shift of the triphenylmethyl dye Coomassie Brilliant Blue G-250 due to complexation with cationic side chains of dissolved enzymes under acidic conditions. As it is only possible to determine the concentration of dissolved species, the immobilized amount onto apatite was calculated by difference between the concentration before and after the 24-h immobilization process. The assay was carried out as described in the standard protocol of Bio-Rad protein assay.

The activity of subtilisin after immobilization is also reported. It was assessed by a "model" bond cleavage reaction on succ-AAPF (succinyl–alanine–alanine–proline–phenylalanine-p-nitroaniline) in 5 mL of 1 M Tris buffer containing 10 mM $CaCl_2$ (pH 7.8); the resulting product p-nitroaniline being quantified photometrically at $\lambda = 405$ nm. The activity of LSZ was also explored via its action live *Micrococcus lysodeikticus* bacterial cells which are lysed in the presence of LSZ (lysis followed by monitoring the optical density at 600 nm). Unfortunately, in this lysozyme case, we were not able to remove completely the apatite particles from the releasing suspension, and the residual presence of some particles would induce a false output on the photometrical read-out; these data are thus not reported here.

Enzyme release was followed at 37 °C in a physiological-like medium (0.1 M HEPES, pH 7.3), as a function of time. The quantification of the released enzymes was performed as above by enzyme titration via Bradford assays.

2.4 Osteogenic cell viability tests

Cell viability was tested via the Neutral Red (NR) colorimetric method [63], a standard cytotoxicity test of the OECD for testing chemicals, performed using the adherent human osteosarcoma cell line CAL-72 (DSMZ no.: ACC 439) which is closely related to normal osteoblasts. Such colorimetric assays are aimed at measuring the vitality of the cells in contact with the tested materials, based on the ability of viable cells to incorporate and bind NR within lysosomes. NR is a cationic dye that readily penetrates the cell membrane and accumulates intracellularly in lysosomes, where it binds to anionic sites of the lysosomal matrix. Changes of the cell surface or the sensitive lysosomal membrane lead to lysosomal fragility and other changes that gradually become irreversible. These alterations result in a decreased uptake and binding of NR. The quantity of dye incorporated into cells is measured by spectrometry (and complementarily by optical microscopy) and is directly proportional to the number of cells with an intact membrane (viable cells), able to incorporate and bind NR within lysosomes.

The assay procedure for testing apatite powder samples was as follows: 500 μL of cell culture medium (commercial DMEM Gibco® Life Technologies) supplemented with 2 mM glutamine (Stock 200 mM), 100 U mL^{-1} penicillin + 100 μg mL^{-1} streptomycin (Stock: 10,000 U mL^{-1} Pen, 10,000 μg mL^{-1} Strep), 1 % insulin, transferrin and selenium (Stock: 100× ITS-G) and 10 % fetal calf serum (all supplements were also provided by Gibco® Life technologies) were added to the apatite samples (with or without enzyme immobilization) and left for desorption of the enzymes for 24 and 48 h respectively at 37 °C. After stabilizing the pH of the medium to 7.5 (by addition, if needed, of a few μL of 1 N NaOH), the osteoblast cells were then incubated with the samples for 24 h. Around 30,000 cells of the CAL-72 cell line were initially seeded in a 96-well MTP and incubated in a cell incubator at 37 °C and 5 % CO_2 overnight for adhesion. After the incubation period of 24 h with the apatite supernatant samples of either 24 or 48 h, the NR tests were carried out. The quantity of the NR dye incorporated into the cells, directly proportional to the number of cells with an intact membrane, was measured by spectrometry (evaluation of optical density, O.D. at 540 nm) after resolving in 200 μL of 1 % Acetic acid in 50 % ethanol.

Tests were also performed on pelletized apatite samples. To ensure that the CAL-72 cells were mostly growing onto the pellets (and not on the surrounding plastic) we used a clone ring (borosilicate glass, provided by Hilgenberg GmbH, Malsfeld, Germany) to restrict their movement. The clone ring was placed onto each of the pellets and 30,000 cells clone^{-1} ring were seeded. These pellets were incubated in the same culture medium as above (supplemented DMEM) at 37 °C with 5 % CO_2. After this incubation period, the supernatant was removed and discarded. Before staining the cells onto the pellets, they were washed with 1,000 μL wel^{-1}l of NR solution I. The cells were afterwards stained with 800 μL well^{-1} with NR (diluted 1:50) for 3 h at 37 °C. Unbound staining solution was removed and the cells were fixed with 800 μL well^{-1} with NR solution II for 5 min. Afterwards, the fixation solution

was removed. To assay the stained cells, a light microscopy was used (VHX-600 and VHX S-15 digital Microscopes, Keyence Deutschland GmbH, Neu-Isenburg, Germany). The cells colored with the NR dye indicated vital cells.

In these cellular assays, the positive control (= good cell viability) consisted in CAL-72 cells simply cultivated in the culture medium (without contact with apatite materials), and the negative control (= poor cell viability) was obtained by treating the CAL-72 cells with cell culture medium containing 0.15 mg mL^{-1} SDS.

2.5 Assessment of antibacterial activity

When mentioned in the text, bacterial growth analyses were carried out. Four strains of particular relevance in the field of nosocomial bone infections, namely Gram-positive *Staphylococcus aureus* and *Staphylococcus epidermidis*, and Gram-negative *Escherichia coli* and *Pseudomonas aeruginosa*, were considered here. The experiments were run in triplicate.

After pre-equilibration in DMEM (1 mL per well in 24-MTP plates) without bacteria for 24 h at 37 °C, the samples were contacted for 24–48 h at 37 °C with the bacteria medium (phosphate-free peptone solution composed of 5 g L^{-1} NaCl and 1 g L^{-1} meat peptone) containing the desired strain of bacteria. The initial number of bacterial cells was ca. 10^8 cfu mL^{-1}. According to the Spread Plate method, a representative part of the supernatant (100 μL) was then extracted and analyzed in a Petri dish on the surface of a nutrient agar plate for bacterial development and quantification: viable bacteria present in the supernatant will form bacterial colonies which represent solitary surviving cells. The linear range of plate count is between 15 and 330 colony forming units per plate (= cfu plate^{-1}). Tenfold dilutions are used in order to yield the cfu in this range. The colonies are numbered macroscopically. This number, the plated volume and the factor of dilution deduce the original number of bacteria in cfu mL^{-1}.

3 Results and discussion

3.1 Physico-chemical characterization of biomimetic calcium-deficient apatite substrates

The apatite samples used in this study were first characterized on a physico-chemical point of view. Their structural and microstructural biomimetic features were confirmed by XRD and FTIR analyses: Fig. 1 shows for example the XRD patterns of apatite samples matured for up to 6 days in comparison with rat bone (9 month-old). Apatite is the unique crystallized phase detectable by XRD for all samples, and the patterns can be indexed using
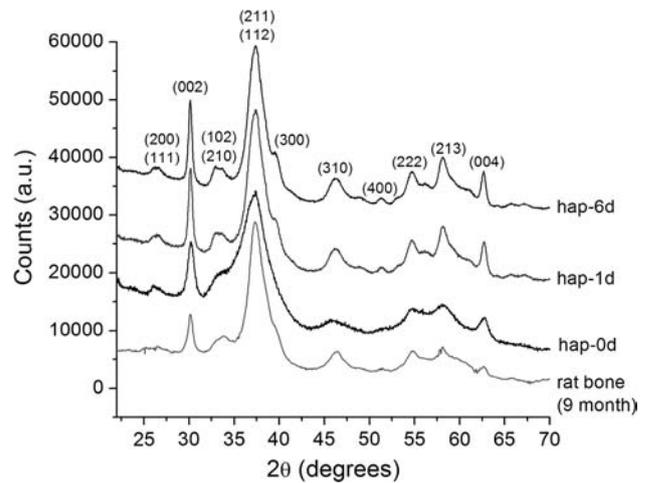

Fig. 1 XRD analysis of biomimetic synthetic apatites prepared in this work, as compared to rat bone (9 months), and indexation with relation to HA (JCPDS 09-432)
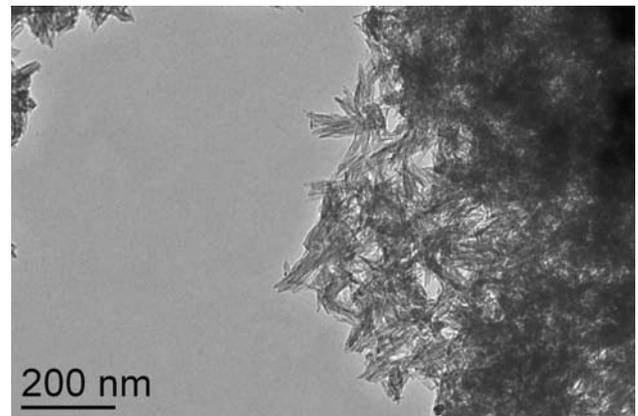

Fig. 2 TEM analysis of a typical biomimetic apatite sample prepared in this work (hap-1d, initial magnification :×20,000)

hydroxyapatite $Ca_{10}(PO_4)_6(OH)_2$ as reference material (JCPDS file 09-432). A clear similarity can be seen with the biological apatite specimen (Fig. 1). Despite a well-known agglomeration phenomenon (macroscopic scale) for apatitic compounds (either biological or synthetic analogs) [64, 65], forming micron-sized polycrystalline aggregates, it is possible to use XRD data to evaluate the dimensions of individual crystals contributing to the XRD pattern (crystallites). The analysis of XRD line broadening by Scherrer's formula applied to lines (002) and (310) then led to the estimation of mean crystallite lengths ranging from 12 to 22 nm and mean widths between 2 and 4.5 nm, for increasing maturation times from 0 to 6 days. These findings confirm that the apatite samples prepared in this work are thus composed of (aggregated) nanosized crystals, as for bone apatites [22]. These nanometer-scale dimensions were also confirmed by TEM observations and Fig. 2 reports the typical case of sample hap-1d.
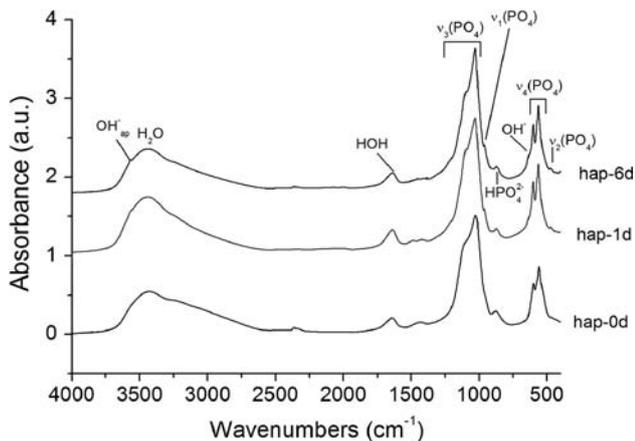
Fig. 3 FTIR spectra for biomimetic synthetic apatites prepared in this work

Fig. 4 Determination of the amount of enzyme stably adsorbed on hap-0d (example of subtilisin) after different washing steps at different pH (phosphate buffer pH 6.5 or Tris buffer pH 7.8)

Fig. 5 Amount of adsorbed subtilisin versus maturation and pH (citrate buffer pH 6.5 or Tris buffer pH 7.8) on apatite powders

Figure 3 reports the FTIR spectra of the prepared apatite samples. The vibrational signature of the samples confirms their apatite nature [22]. Moreover, the presence of a band around 870 cm^{-1}, characteristic of HPO_4^{2-} ions, and the rather low intensity of the OH$^-$ band (especially the OH libration band at 632 cm^{-1} which only appears as a shoulder to the $\nu_3(PO_4)$ band) are two other elements pointing out the bone-like character of these compounds [66, 67].

Chemical analyses carried out on these biomimetic apatite samples led to Ca/P molar ratios ranging from 1.35 to 1.47 for maturations times from 0 to 6 days. These values, although increasing with maturation time, are significantly lower than the value of 1.67 found for stoichiometric hydroxyapatite, which points out the nonstoichiometric character of these apatite compounds. Such low Ca/P ratios are also found in biological apatites constitutive of bone mineral [22, 67], stressing again the similarity of such samples with bone apatite.

3.2 Immobilization of enzymes on apatite substrates

In a first step, the amount of enzymes stably adsorbed on the apatite substrates (characterized by a BET surface area of the order of 100 m^2 g^{-1}) in our experimental conditions was evaluated. Our data indicated that 40–60 % of the amount of enzymes initially associated to the apatite phase during the immersion process (see protocol details in experimental section) were stably adsorbed on the apatite substrate, as the remaining molecules could be easily washed away during the washing process. This is illustrated on Fig. 4 in the case of subtilisin (not yet reported in interaction with apatite to our knowledge) on hap-0d. The effectiveness of the washing process was determined by way of repeated enzyme titrations by Bradford assays. The stabilization of the amounts of immobilized enzymes at this stage (three washing steps were found to be adequate) allowed us to consider that the
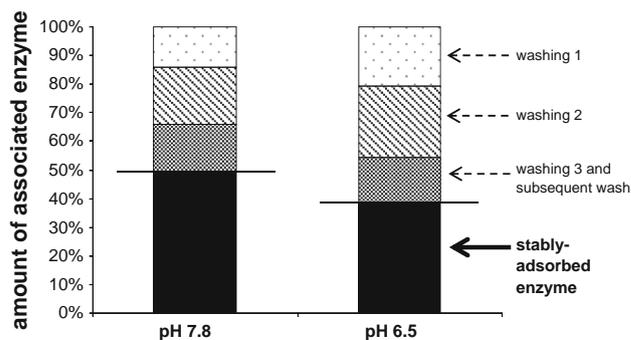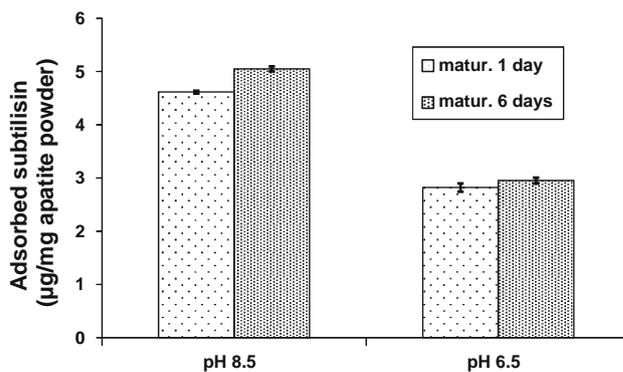
adsorption equilibrium had then been reached (adsorbed amounts corresponding to steady adsorption values, Fig. 5). It was also noted that the maturation time of the apatite—tested here in the range 0–6 days—had only a minor effect on the amount of immobilized enzyme, which is illustrated in Fig. 5 by comparing subtilisin adsorption on hap-1d and hap-6d. Taking into account this low impact of initial maturation time on the interaction with the enzymes tested, this parameter will thus not be systematically recalled in the rest of this paper.

On the other hand, adsorbed amounts were systematically found to be greater at pH 7.8 rather than in more acidic conditions (pH 6.5), whether the adsorption was performed on apatite powders (Fig. 5) or on pellets (Fig. 6). This behavior can be linked to various cumulative phenomena: one explanation could be the stronger competitive adsorption between enzyme molecules and ions contained in the pH 6.5-buffers (i.e. citrate or phosphate ions, since such molecular ions are known to interact rather well with apatitic surface [68]), thus leading in turn to a lower number of accessible adsorption sites for enzymes. Furthermore, more acidic media are likely to alter the surface of apatite nanocrystals (accelerated partial dissolution or modification of the
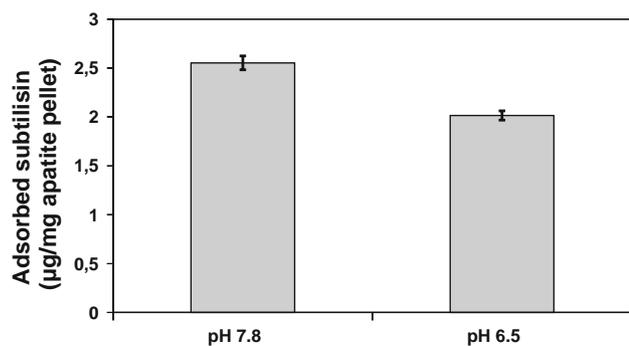
Fig. 6 Amount of adsorbed subtilisin versus pH (citrate buffer pH 6.5 or Tris buffer pH 7.8) on apatite pellets

Fig. 7 Assessment of immobilized enzyme activity in U mg^{-1} powder (case of subtilisin) on hap-0d

composition of the hydrated surface layer) thus modifying adsorption capabilities. Finally, the conformation and overall charge of the enzyme itself may also vary depending on the pH of the medium: indeed, a pH value below the isoelectric point of a protein tends to favor a positive total charge (by favoring –NH^{3+} and –COOH end-groups on the constitutive amino acids) whereas a pH above the isoelectric point favors a negative charge (favored –NH$_2$ and –COO$^-$ groups). In the case of hydroxyapatite, the overall surface charge gets slightly negative for pH values above ca. 7 whereas it becomes less negative or even positive as pH drops below this value [69]. The subtilisin and LSZ used in this work have an isoelectric point (pI) of 8.7 and 9.2 respectively. Therefore, they are bound to exhibit a global positive charge in both buffers (6.5 and 7.8). They are thus likely to interact more strongly when HA-like surfaces are globally negative, i.e. at pH values between 7 and their pI, which is the case for the immobilization protocol run in Tris buffer (pH 7.8). This surface charge aspect could thus contribute to the greater adsorbed amount observed at pH 7.8 as compared to pH 6.5. A more detailed examination of the surface charge of nanocrystalline apatites will however be needed (future work) to explore this point in more details.

Additional experiments were then run to ensure that such immobilized enzymes kept a biological activity, even after drying. This was indeed confirmed for subtilisin by obtaining significant levels of activity (Fig. 7), of the order of 240–280 U mg^{-1} at both pH values, as checked by a "model" bond cleavage reaction with succ-AAPF (quantification followed by photometric quantification at $\lambda = 405$ nm, see experimental section), even after treatment of the apatite compounds for 3 h at 50 °C. The immobilization and the drying processes were thus found to preserve enzymatic functions, which can probably be extrapolated to other enzymes fixed on apatite surfaces. This conserved enzymatic activity may probably be related to the release of the enzyme in the surrounding solution followed by the expected molecular interaction with the succ-AAPF reactant. The non-alteration of this activity,
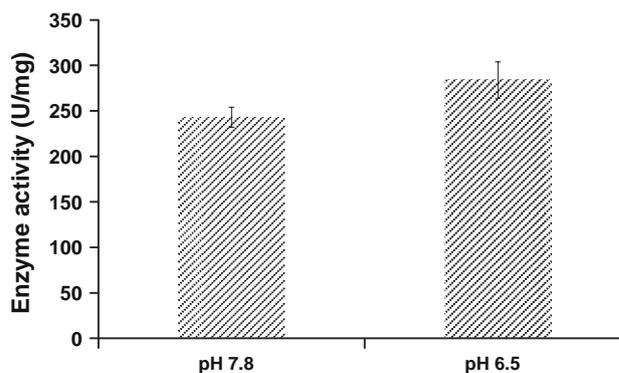
even after drying, then substantiates the fact that possible galenic/pharmaceutical formulations involving such hybrid enzyme/biomimetic apatite systems could indeed be prepared and potentially used in biomedical applications.

Enzyme release experiments were then carried out at this stage, at 37 °C in HEPES medium (pH 7.3), for directly illustrating the possibility to liberate such adsorbed molecules from apatite nanocrystal surfaces. Figure 8a shows the release profile obtained in the case of LSZ immobilized at pH 7.8 in Tris buffer on nanocrystalline apatite (hap-1d pellet). In this experiment, an initial LSZ loading of ∼1.1 µg mg^{-1} was used. The obtained cumulative profile shows that the release from the nanocrystalline apatite surface is initiated as soon as the re-immersion starts, without significant latent time. It may be added that experiments performed on samples for which the immobilization had been carried out at pH 6.5 (citrate buffer) showed a similar trend, only with a slower stabilization (the 100 % release was reached after about 8 days compared to 3 days for pH 7.8), and this different behavior depending on the initial immobilization pH can probably be related to the change in surface features of the apatite (see previous discussion), although at this point it is difficult to give more detailed mechanistic explanations. It can be remarked from Fig. 8a, as could be expected from this surface-only doping situation, that this type of release profile cannot be satisfactorily fitted as a Fickian rate (rate proportional to $\sqrt{t}$) which is more adapted to diffusional mechanisms (the process being significantly faster here). This fast release behavior is instead indicative of rather weak interaction forces between apatite nanocrystals and the adsorbed enzyme molecules. A variation in affinity of amino-acids for apatite surfaces, depending on exposed ionic end-groups, has been described in the literature for adsorptive processes: for example, serine adsorption was found to be significantly weaker than phospho-serine adsorption [70]. The chemical composition of the enzyme itself is thus expected to play a role in the modulation of
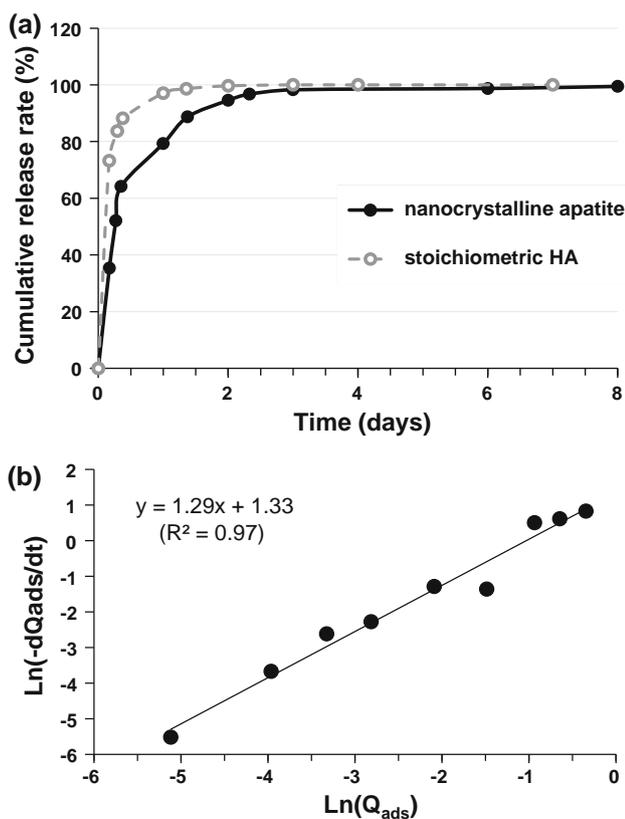
Fig. 8 a Lysozyme release study in HEPES pH 7.3 at 37 °C (immobilization performed in Tris buffer at pH 7.8 on nanocrystalline apatite and on stoichiometric HA), and **b** linearization data (case of nanocrystalline apatite)

adsorptive forces in such systems. To some extent, the surface features of the apatite substrate are also likely to have an impact on the release profile. This was for example illustrated here by carrying out the same release experiment but using stoichiometric HA as substrate. In this case (see Fig. 8a), even faster release kinetics were evidenced. This behavior can probably be explained by differences in surface state between nonstoichiometric apatite nanocrystals and (micron-sized) stoichiometric hydroxyapatite crystals. Indeed, previous studies have shown that biomimetic apatite nanocrystals were covered by a non-apatitic ionic surface layer with very labile ions (see for example refs. [14, 24, 71]), and this matter of fact may then lead to somewhat enhanced adsorption properties.

Despite a release pattern slower for biomimetic apatite than for stoichiometric HA, the kinetics remain fast in all cases. In this context, this release of LSZ molecules can probably be described here on the basis of a "simple" desorption process out of the apatite surface, without complex diffusion aspects or simultaneous ion exchange processes (in contrast to the case of stronger adsorption processes such as bisphosphonate adsorption for example [29]). In this scenario, which becomes then identical for

example to the desorption of chemisorbed gaseous molecules from solid surfaces (widely described in scientific textbooks), the rate of desorption "r_d" can be written as follows:

$$r_d = -\frac{dQ_{ads}(t)}{dt} = \alpha \cdot [Q_{ads}(t)]^m \cdot \exp\left(-\frac{E_d}{RT}\right) \qquad (1)$$

where $Q_{ads}(t)$ is the remaining adsorbed amount at time t (which is thus an indication of the coverage of the surface by the molecule), "α" is the pre-exponential factor, "m" is the order of the desorption kinetics, and E_d is the activation energy of the desorption process. In this equation, the value of "m" is in particular informative on the nature of the elementary steps that govern the desorption phenomenon. Two specific values of "m" are often encountered in the literature: $m = 1$ or 2, for kinetic rules of order 1 and 2, respectively. While a non-dissociative "molecular" desorption process is generally found to be of order 1, dissociative events often lead to order 2 kinetics or to more complex behaviors. In practice, the value of "m" can be evaluated from the slope of the curve $\mathrm{Ln}(-dQ_{ads}/dt) = f(\mathrm{Ln}Q_{ads})$. In the present case (see Fig. 8b), this linearization step led to $m \approx 1.29$. The closeness of this value to unity appears in perfect agreement with a straightforward molecular desorption of the enzyme with time, where the release rate is proportional to the remaining coverage. This data analysis had not been reported previously, but authors suggested from their adsorption data that LSZ adsorption on apatitic surfaces was a simple electrostatic mechanism with an unhindered release upon dilution [42]. Our data thus suggest that this situation is also true for nanocrystalline apatite surfaces for which the biomimetic character was evidenced.

Although stronger affinities are likely to be noticed at the occasion of future studies—not yet initiated—with other enzymes (exhibiting various types of chemistry, conformation etc.) or even upon modification of the apatite substrate itself, the above results suggest that enzyme/biomimetic apatite materials may find applicative perspectives in medicine, for example in cases when a non-delayed release is desirable: e.g. for rapidly initiating some enzymatic pathways at the site of implantation, or else for promptly fighting against post-surgical invading microorganisms (possibly in synergy with another antimicrobial agent that would be released in a more delayed way), among other applications.

3.3 Human cell viability results

Optical microscopy observations indicated that the CAL-72 osteoblastic cells (human origin) were able to adhere on such nanocrystalline apatite substrates. The presence or absence of enzymes had no apparent effect on cell adhesion behavior. It was noted that—independently on the presence
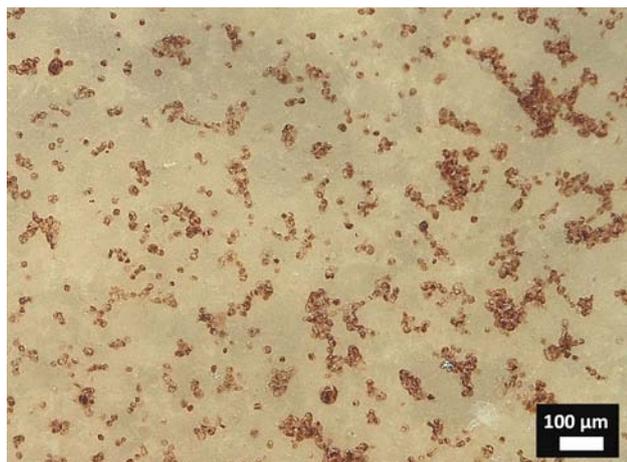
Fig. 9 CAL-72 cells directly cultivated on unfunctionalized-apatite pellet

Fig. 10 Cell viability assessment (NR testing) for cell controls, unfunctionalized and lysozyme-functionalized apatite (pH 6.5: 1.29 μg mg^{-1} and pH 7.8: 1.05 μg mg^{-1})

or absence of immobilized enzymes—the cells formed rather isolated islands or clusters instead of a uniform packed monolayer (Fig. 9): this observation can most probably be related to the high porosity of the samples studied in this work (mesoporous materials, especially with a typical mesopore size distribution around 25 nm as determined from BJH-plots).

In all cases, the enzyme-functionalized apatite samples tested in this work were found—as for unfunctionalized apatites—to be non-cytotoxic to the CAL-72 osteoblast cells, and this was found to be independent of the samples shape (whether as powders or pellets). This is for example illustrated by Fig. 10. This absence of cytotoxicity can be considered as a first interesting feature when considering the use of such nanocrystalline apatite compounds and their associations with enzymatic entities in biomedical applications, especially in relation with bone tissue engineering.

3.4 Behavior towards bacterial cells

The results above indicated that controlled associations (via surface functionalization) of enzyme species and nanocrystalline biomimetic calcium-deficient apatites were experimentally feasible. Moreover, the activity of such immobilized enzymes in terms of enzymatic bond cleavage ability was conserved (as illustrated above by the "model" transformation of succ-AAPF into p-nitroaniline). It was thus interesting at this point to explore also other potential aspects of enzyme activity, such as antibacterial properties.

As mentioned in the introductive section, LSZ is for instance known to interact and potentially damage bacterial cell walls, particularly on Gram-positive bacteria. It was therefore appealing to determine whether such an antibacterial activity could also be confirmed in the present study based on our biomimetic apatite/LSZ hybrids.
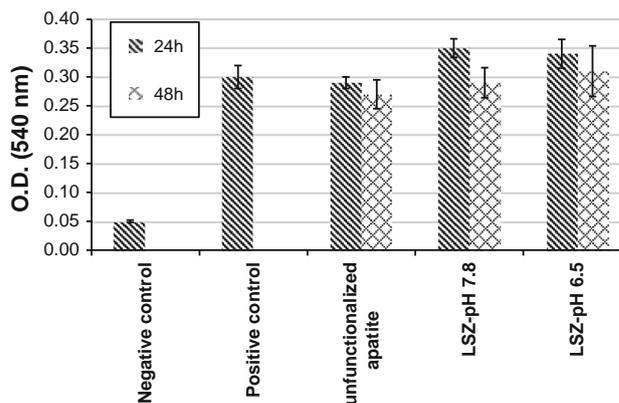
To this aim, we investigated the potential antibacterial properties of LSZ-functionalized apatite (initial loading of the pellets close to 1 μg mg^{-1} in either Tris or Citrate buffer; experimental values: 1.05 and 1.29 μg mg^{-1} respectively). This study was performed on four different bacterial strains of relevance in bone infections: *S. aureus*, *S. epidermidis*, both Gram-positive, and *E. coli* and *P. aeruginosa*, both Gram-negative. Apatite samples (hap-1d pellets) were contacted with these strains prior to bacterial quantification, following experimental procedures detailed in the experimental section.

Results relating to the quantification of the number of bacterial colonies present in the supernatant showed no significant effect on *E. coli* or *P. aeruginosa* microorganisms (Fig. 11), as the number of cfu mL^{-1} was found to be essentially identical to the bacterial control (bacteria alone). These findings thus indicated an absence of noticeable antibacterial activity towards such the tested Gram-negative bacteria, at least in our experimental conditions. Lower activity of lysozyme towards Gram-negative bacteria has indeed been previously reported although this point is still a matter of controversy [72, 73].

In contrast, a noticeable reduction in the number of colonies of *S. aureus* and *S. epidermidis* (Gram-positive) was observed as shown in Fig. 11. It can be noted that this antibacterial property was found to be even more pronounced when the LSZ functionalization had been performed at close-to-physiological pH (Tris buffer, pH 7.8) rather than in acidic conditions (citrate buffer, pH 6.5). This may possibly be attributable to the faster release observed for pH 7.8, which may in turn be related to a variation of apatite nanocrystal surface characteristics as a function of pH [17] thus modifying adsorption/desorption processes. The experimental data show, as illustrated in Fig. 11, a reduction in cfu mL^{-1} numbers reaching -99.3 % for *S. epidermidis* and -98.8 % for *S. aureus*.

Fig. 11 Bacterial cells behavior for lysozyme-functionalized apatite (prepared in Tris buffer pH 7.8 or citrate buffer pH 6.5) and for the control (bacteria alone, O.D. 0.05)
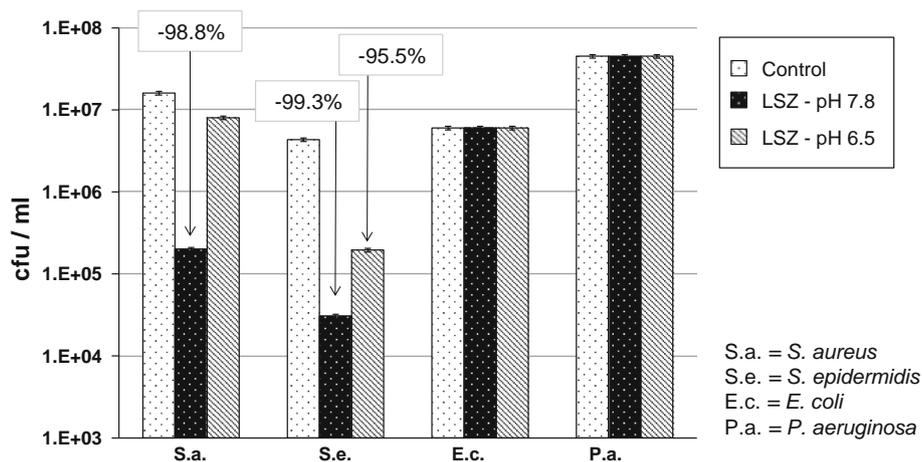
Although the main objective of this paper was to show the feasibility of biomimetic apatite/enzyme associations and not to explore in depth the antimicrobial potentialities of such hybrid systems, these findings demonstrate that immobilized enzymes not only retain enzymatic activity towards "model" cleavage reactions but also regarding more "applied" aspects such as antibacterial properties for bone-intended bioceramics, thus opening a wide range of biomedical perspectives.

3.5 Concluding remarks

In this contribution we showed, on an experimental basis, that associations of enzymes and *biomimetic* calcium-deficient apatite compounds were feasible in a material-making objective. This was possible while retaining the biological activity of the immobilized enzymes (even after drying), which we illustrated here by enzymatic bond cleavage process and antibacterial properties. Biological features of such hybrid compounds were then investigated in view of a possible use in bone surgery. They were shown to be non-cytotoxic toward mammalian cells such as human osteoblast-like CAL-72 cells and potentially promising for antimicrobialness, for instance toward Gram-positive strains such as *S. aureus* or else *S. epidermidis* that are relevant strains especially in bone post-surgical events.

Beyond the specific examples discussed in this work, the idea of enzyme/biomimetic apatite combinations could thus be seen as real material-making systems, opening applicative perspectives in the treatment of some pathologies (e.g. nosocomial bone infections) or for the reinforcement or activation of localized enzymatic reactions. The very versatile character of such associations, exploiting the surface reactivity of *nanocrystalline apatite* nanocrystals for a functionalization with a *variety of potential enzymes*, appears consequently as particularly favorable for the design of new biotechnological tools.

References

1. López-Macipe A, Gómez-Morales J, Rodríguez-Clemente R. Nanosized hydroxyapatite precipitation from homogeneous calcium/citrate/phosphate solutions using microwave and conventional heating. Adv Mater. 1998;10:49.
2. Tas AC. Synthesis of biomimetic Ca-hydroxyapatite powders at 37 °C in synthetic body fluids. Biomaterials. 2000;21:1429–38.
3. Chai CS, Ben-Nissan B. Bioactive nanocrystalline sol–gel hydroxyapatite coatings. J Mater Sci. 1999;10:465–9.
4. Guo XY, Gough JE, Xiao P, Liu J, Shen ZJ. Fabrication of nanostructured hydroxyapatite and analysis of human osteoblastic cellular response. J Biomed Mater Res A. 2007;82A:1022–32.
5. Yeong KCB, Wang J, Ng SC. Mechanochemical synthesis of nanocrystalline hydroxyapatite from CaO and CaHPO4. Biomaterials. 2001;22:2705–12.
6. Rameshbabu N, Rao KP, Kumar TSS. Acclerated microwave processing of nanocrystalline hydroxyapatite. J Mater Sci. 2005;40:6319–23.
7. Nassif N, Martineau F, Syzgantseva O, Gobeaux F, Willinger M, Coradin T, Cassaignon S, Azaïs T, Giraud-Guille MM. In vivo inspired conditions to synthesize biomimetic hydroxyapatite. Chem Mater. 2010;22:3653–63.
8. Iafisco M, Marchetti M, Gómez-Morales J, Hernández-Hernández MA, García-Ruiz JM, Roveri N. Silica gel template for calcium phosphates crystallization. Cryst Growth Des. 2009;9:4912–21.
9. Phillips MJ, Darr JA, Luklinska ZB, Rehman I. Synthesis and characterization of nano-biomaterials with potential osteological applications. J Mater Sci. 2003;14:875–82.
10. San Thian E, Ahmad Z, Huang J, Edirisinghe MJ, Jayasinghe SN, Ireland DC, Brooks RA, Rushton N, Bonfield W, Best SM. The role of electrosprayed apatite nanocrystals in guiding osteoblast behaviour. Biomaterials. 2008;29:1833–43.
11. Drouet C. Apatite formation: why it may not work as planned, and how to conclusively identify apatite compounds. BioMed Res

Int. 2013;2013:1–12. doi:10.1155/2013/490946 (Article ID 490946).

12. Bertinetti L, Drouet C, Combes C, Rey C, Tampieri A, Coluccia S, Martra G. Surface characteristics of nanocrystalline apatites: effect of Mg surface enrichment on morphology, surface hydration species, and cationic environments. Langmuir. 2009;25:5647.

13. Drouet C, Carayon M, Combes C, Rey C. Exchange of biologically relevant ions on nanocrystalline apatites. Geochim Cosmochim Acta. 2005;69:A69.

14. Drouet C, Carayon M, Combes C, Rey C. Surface enrichment of biomimetic apatites with biologically-active ions Mg2+ and Sr2+: a preamble to the activation of bone repair materials. Mater Sci Eng C. 2008;28:1544.

15. Grossin D, Rollin-Martinet S, Estournes C, Rossignol F, Champion E, Combes C, Rey C, Chevallier G, Drouet C. Biomimetic apatite sintered at very low temperature by spark plasma sintering: physico-chemistry and microstructure aspects. Acta Biomaterialia. 2010;6:577.

16. Sakhno Y, Bertinetti L, Iafisco M, Tampieri A, Roveri N, Martra G. Surface hydration and cationic sites of nanohydroxyapatites with amorphous or crystalline surfaces: a comparative study. J Phys Chem C. 2010;114:16640.

17. Vandecandelaere N, Rey C, Drouet C. Biomimetic apatite-based biomaterials: on the critical impact of synthesis and post-synthesis parameters. J Mater Sci. 2012;23:2593.

18. Jager C, Welzel T, Meyer-Zaika W, Epple M. A solid-state NMR investigation of the structure of nanocrystalline hydroxyapatite. Magn Reson Chem. 2006;44:573–80.

19. Al-Kattan A, Dufour P, Dexpert-Ghys J, Drouet C. Preparation and physicochemical characteristics of luminescent apatite-based colloids. J Phys Chem C. 2010;114:2918.

20. Al-Kattan A, Girod-Fullana S, Charvillat C, Ternet-Fontebasso H, Dufour P, Dexpert-Ghys J, Santran V, Bordere J, Pipy B, Bernad J, Drouet C. Biomimetic nanocrystalline apatites: emerging perspectives in cancer diagnosis and treatment. Int J Pharm. 2012; 423:26.

21. Mondejar SP, Kovtun A, Epple M. Lanthanide-doped calcium phosphate nanoparticles with high internal crystallinity and with a shell of DNA as fluorescent probes in cell experiments. J Mater Chem. 2007;17:4153.

22. Gómez-Morales J, Iafisco M, Delgado-López JM, Sarda S, Drouet C. Progress on the preparation of nanocrystalline apatites and surface characterization: overview of fundamental and applied aspects. Prog Cryst Growth Charact Mater. 2013;59:1–46.

23. Eichert D, Drouet C, Sfihi H, Rey C, Combes C. Nanocrystalline apatite-based biomaterials: synthesis, processing and characterization. In: Kendall JB, editor. Biomaterials research advances. New York: Nova Science; 2007. p. 93–143.

24. Eichert D, Combes C, Drouet C, Rey C. Formation and evolution of hydrated surface layers of apatites. Bioceramics. 2005;17:3.

25. Cazalbou S, Eichert D, Ranz X, Drouet C, Combes C, Harmand MF, Rey C. Ion exchanges in apatites for biomedical application. J Mater Sci. 2005;16:405.

26. Ouizat S, Barroug A, Legrouri A, Rey C. Adsorption of bovine serum albumin on poorly crystalline apatite: influence of maturation. Mater Res Bull. 1999;34:2279.

27. Midy V, Rey C, Bres E, Dard M. Basic fibroblast growth factor adsorption and release properties of calcium phosphate. J Biomed Mater Res. 1998;41:405.

28. Autefage H, Briand-Mesange F, Cazalbou S, Drouet C, Fourmy D, Goncalves S, Salles J, Combes C, Swider P, Rey C. Adsorption and release of BMP-2 on nanocrystalline apatite-coated and uncoated hydroxyapatite/beta-tricalcium phosphate porous ceramics. J Biomed Mater Res B. 2009;91B:706–15.

29. Errassifi F, Menbaoui A, Autefage H, Benaziz L, Ouizat S, Santran V, Sarda S, Lebugle A, Combes C, Barroug A, Sfihi H, Rey C. Adsorption on apatitic calcium phosphates: applications to drug delivery. Adv Bioceram Biotechnol. 2010;218:159.

30. Barroug A, Kuhn LT, Gerstenfeld LC, Glimcher MJ. Interactions of cisplatin with calcium phosphate nanoparticles: in vitro controlled adsorption and release. J Orthop Res. 2004;22:703.

31. Gaudin A, Jacqueline C, Gautier H, Desessard C, Le Mabecque V, Miegeville AF, Potel G, Bouler JM, Weiss P, Caillon J, Amador G. A delivery system of linezolid to enhance the MRSA osteomyelitis prognosis: in vivo experimental assessment. Eur J Clin Microbiol Infect Dis. 2013;32:195.

32. Bosco R, Iafisco M, van den Beucken J, Leeuwenburgh S, Jansen J. Adsorption of alendronate onto biomimetic apatite nanocrystals to develop drug carrier coating for bone implants. Key Eng Mater. 2013;529–530:475–9.

33. Sharma R, Pandey RR, Gupta AA, Kar S, Dhayal M. In situ amino acid functionalization and microstructure formation of hydroxyapatite nanoparticles synthesized at different pH by precipitation route. Mat Chem Phys. 2012;133:718–25.

34. Lebugle A, Rodrigues A, Bonnevialle P, Voigt JJ, Canal P, Rodriguez F. Study of implantable calcium phosphate systems for the slow release of methotrexate. Biomaterials. 2002;23:3517–22.

35. Ginebra MP, Canal C, Espanol M, Pastorino D, Montufar EB. Calcium phosphate cements as drug delivery materials. Adv Drug Deliv Rev. 2012;64:1090–110.

36. Josse S, Faucheux C, Soueldan A, Grimandi G, Massiot D, Alonso B, Janvier P, Laib S, Pilet P, Gauthier O, Daculsi G, Guicheux J, Bujoli B, Bouler JM. Novel biomaterials for bisphosphonate delivery. Biomaterials. 2005;26:2073–80.

37. Hayakawa S, Ando K, Tsuru K, Osaka A. Structural characterization and protein adsorption property of hydroxyapatite particles modified with zinc ions. J Am Ceram Soc. 2007;90:565–9.

38. IafiscoM, Palazzo B, Marchetti M, Margiotta N, Ostuni R, Natile G, Morpurgo M, Gandin V, Marzano C, Roveri N. Smart delivery of antitumoral platinum complexes from biomimetic hydroxyapatite nanocrystals. J Mater Chem. 2009;19:8385–92.

39. Hu YY, Rawal A, Schmidt-Rohr K. Strongly bound citrate stabilizes the apatite nanocrystals in bone. PNAS. 2010;107: 22425–9.

40. Al-Kattan A, Errassifi F, Sautereau AM, Sarda S, Dufour P, Barroug A, Dos Santos I, Combes C, Grossin D, Rey C, Drouet C. Medical potentialities of biomimetic apatites through adsorption, ionic substitution, and mineral/organic associations: three illustrative examples. Adv Eng Mater. 2010;12:B224–33.

41. Hafiz Uddin M, Matsumoto T, Ishihara S, Nakahira A, Okazaki M, Sohmura T. Apatite containing aspartic acid for selective protein loading. Dent Res. 2010;89:488–92.

42. Barroug A, Lemaitre J, Rouxhet PG. Lysozyme on apatite—a model of protein adsorption controlled by electrostatic interactions. Colloids Surf. 1989;37:339.

43. Akazawa T, Kobayashi M, Kanno T, Kodaira K. Discrimination of albumin and lysozyme-adsorption characteristics on two differently-originated apatites. Chem Lett. 1996;9:779.

44. Akazawa T, Kobayashi M, Kanno T, Kodaira K. Characterization of albumin- and lysozyme adsorption evaluated on two differently prepared apatites. J Mater Sci. 1998;33:1927.

45. Kanno T, Sendai T, Tada K, Horiuchi J, Akazawa T, Itabashi K. Desorption properties of BSA and LSZ on carbonate ion-modified apatite. J Ceram Soc Jpn. 2009;117:1101.

46. Martins AM, Pereira RC, Leonor IB, Azevedo HS, Reis RL. Chitosan scaffolds incorporating lysozyme into CaP coatings produced by a biomimetic route: a novel concept for tissue engineering combining a self-regulated degradation system with in situ pore formation. Acta Biomater. 2009;5:3328.

47. Martins AM, Pham QP, Malafaya PB, Raphael RM, Kasper FK, Reis RL, Mikos AG. Natural stimulus responsive scaffolds/cells for bone tissue engineering: influence of lysozyme upon scaffold

degradation and osteogenic differentiation of cultured marrow stromal cells induced by CaP coatings. Tissue Eng Part A. 2009; 15:1953.

48. Li J, Shirosaki Y, Hayakawa S, Stamboulis A, Osaka A. Sol-gel preparation of apatite-coated silica macrospheres from water glass and their adsorption of bovine serum albumin and lysozyme. J Ceram Soc Jpn. 2012;120:355.

49. Lee WH, Loo CY, Van KL, Zavgorodniy AV, Rohanizadeh R. Modulating protein adsorption onto hydroxyapatite particles using different amino acid treatments. J R Soc Interface. 2012;9:918.

50. Mueller B, Zacharias M, Rezwan K. Bovine serum albumin and lysozyme adsorption on calcium phosphate particles. Adv Eng Mater. 2010;12:B53–61.

51. Roger V, Tenovuo J, Lenanderlumikari M, Soderling E, Vilja P. Lysozyme and Lactoperoxidase inhibit the adherence of streptococcus-mutans NCTC-10449 (Serotype-C) to saliva-treated hydroxyapatite in vitro. Caries Res. 1994;28:421.

52. Gujral MS, Patnaik PM, Kaul R, Parikh HK, Conradt C, Tamhankar CP, Daftary GV. Efficacy of hydrolytic enzymes in preventing radiation therapy-induced side effects in patients with head and neck cancers. Cancer Chemother Pharmacol. 2001;47:S23.

53. Millan CG, Marinero MLS, Castaneda AZ, Lanao JM. Drug, enzyme and peptide delivery using erythrocytes as carriers. J Controlled Release. 2004;95:27.

54. Marchesan D, Cox TM, Deegan PB. Lysosomal delivery of therapeutic enzymes in cell models of Fabry disease. J Inherit Metab Dis. 2012;35:1107.

55. Sangeetha K, Morris VB, Abraham TE. Stability and catalytic properties of encapsulated subtilisin in xerogels of alkoxisilanes. Appl Catal A. 2008;341:168.

56. Veluchamy P, Sivakumar PM, Doble M. Immobilization of subtilisin on polycaprolactam for antimicrobial food packaging applications. J Agric Food Chem. 2011;59:10869.

57. Abergel C, Monchois V, Byrne D, Chenivesse S, Lembo F, Lazzaroni JC, Claverie JM. Structure and evolution of the Ivy protein family, unexpected lysozyme inhibitors in Gram-negative bacteria. Proc Natl Acad Sci USA. 2007;104:6394.

58. Hangler M, Burmolle M, Schneider I, Allermann K, Jensen B. The serine protease Esperase HPF inhibits the formation of multispecies biofilm. Biofouling. 2009;25:667.

59. Fleming A. On a remarkable bacteriolytic element found in tissues and secretions. Proc R Soc Lond Series B-Contain Papers Biologic Character. 1922;93:306.

60. Newman J, Josephso As, Cacatian A, Tsang A. Spinal-fluid lysozyme in diagnosis of central-nervous-system tumors. Lancet. 1974;2:756.

61. Charlot G. Chimie analytique quantitative, vol. 2. Paris: Masson; 1974.

62. Norde W, Anusiem ACI. Adsorption, desorption and readsorption of proteins on solid surfaces. Colloids Surf. 1992;66:73.

63. Borenfreund E, Puerner JA. Toxicity determined in vitro by morphological alterations and neutral red absorption. Toxicol Lett. 1985;24:119–24.

64. Sato K, Hotta Y, Nagaoka T, Yasuoka M, Watari K. Agglomeration control of hydroxyapatite nanocrystals grown in phase-separated microenvironments. J Mater Sci. 2006;41:5424–8.

65. Dorozhkin SV. Nanodimensional and nanocrystalline calcium orthophosphates. Int J Chem Mater Sci. 2013;1:105–74.

66. Rey C, Lian J, Grynpas M, Shapiro F, Zylberberg L, Glimcher MJ. Non-apatitic environments in bone mineral: FT-IR detection, biological properties and changes in several disease states. Connect Tissue Res. 1989;21:267–73.

67. Rey C, Hina A, Tofighi A, Glimcher MJ. Maturation of poorly crystalline apatites: chemical and structural aspects in vivo and in vitro. Cells Mater. 1995;5:345.

68. Delgado-Lopez JM, Iafisco M, Rodriguez I, Tampieri A, Prat M, Gomez-Morales J. Crystallization of bioinspired citrate-functionalized nanoapatite with tailored carbonate content. Acta Biomater. 2012;8:3491.

69. Somasundaran P, Markovic B. Interfacial properties of calcium phosphates. In: Amjad Z, editor. Calcium phosphates in biological and industrial systems, vol. 5. Dordrecht: Kluwer Academic; 1998.

70. Benaziz L, Barroug A, Legrouri A, Rey C, Lebugle A. Adsorption of O-phospho-L-serine and L-serine onto poorly crystalline apatite. J Colloid Interface Sci. 2001;238:48.

71. Drouet C, Gómez-Morales J, Iafisco M, Sarda S. Calcium phosphate surface tailoring technologies for drug delivering and tissue engineering and applied aspects. In: Rimondini L, Bianchi CL, Vernè E, editors. Surface tailoring of inorganic materials for biomedical applications. Dubai: E-book: Bentham Science; 2012. p. 43–111.

72. Derde M, Lechevalier V, Guerin-Dubiard C, Cochet MF, Jan S, Baron F, Gautier M, Vie V, Nau F. Hen egg white lysozyme permeabilizes escherichia coli outer and inner membranes. J Agroic Food Chem. 2013;61:9922–9.

73. Takada K, Ohno N, Yadomae T. Detoxification of lipopolysaccharide (LPS) by egg white lysozyme. FEMS Immunol Med Microbiol. 1994;9:255–63.